Supplementary Material

Effect of the Crystal Structure on the Piezoelectricity of [001]-Textured (Na, K)(Nb, Sb)O_3-$SrZrO_3$-(Bi, Ag)ZrO_3 Lead-Free Piezoelectric Thick Film

Su-Hwan Go [1], Dae-Su Kim [1], Yeon-Gyeong Chae [1], Seok-June Chae [1], Eun-Ji Kim [1], Hyeon-Min Yu [1], Bum-Joo Kim [1], Seok-Jung Park [1], Joun-Ho Lee [2] and Sahn Nahm [1,*]

[1] Department of Materials Science and Engineering, Korea University, Seoul 02841, Republic of Korea
[2] Foundation Lab, LG Display Co., Ltd., Seoul 07796, Republic of Korea
* Correspondence: snahm@korea.ac.kr; Tel.: +82-2-3290-3279

1. Synthesis and measurement of the structural, piezoelectric, dielectric, and ferroelectric properties of NKNS-(0.04-x)SZ-xBAZ + *y* mol% NN thick films

***Synthesis*:** $0.96(Na_{0.5}K_{0.5})(Nb_{0.93}Sb_{0.07})O_3$-(0.04-x)$SrZrO_3$-x$(Bi_{0.5}Ag_{0.5})ZrO_3$ [NKNS-(0.04-x)SZ-xBAZ] ceramic powders ($0.0 \leq x \leq 0.04$) were prepared using a conventional solid-state method. Na_2CO_3, K_2CO_3, Nb_2O_5, Sb_2O_3, $SrCO_3$, ZrO_2, Bi_2O_3, and Ag_2O precursors (>99%, High Purity Chemicals, Saitama, Japan) were weighed (total, 20.0 g) and mixed by ball milling for 24 h in a Nalgene bottle (250 mL) containing anhydrous ethanol (35.0 mL) and yttria-stabilized zirconia (YSZ) balls. The quantities of Na_2CO_3 and Nb_2O_5 in the precursor powder of NKNS-(0.04-x)SZ-xBAZ were adjusted (i.e., decreased) because the NN seeds diffused into the ceramic matrix during sintering. After ball milling, the powder mixtures were dried and then calcined at 850 °C for 3 h. Subsequently, the calcined powders were ball milled for 72 h with 0.5 mol% Fe_2O_3 as a sintering aid (>95%, Kanto Chemical, Japan).

Characterization: The crystal structure and degree of texturing of the samples were investigated by X-ray diffraction (XRD; Shimadzu, XRD-6100). The degree of texturing in the samples was determined using the Lotgering factor (LF), which can be calculated using the following equation [1, 2]:

$$LF = \frac{P-P_0}{1-P_0}, \text{ where } P = \frac{\sum I_{T(00l)}}{\sum I_{T(hkl)}} \text{ and } P_0 = \frac{\sum I_{R(00l)}}{\sum I_{R(hkl)}}, \qquad \text{(Eq. S1)}$$

where $I_{R(hkl)}$ and $I_{T(hkl)}$ are the intensities of the (*hkl*) reflections for the randomly oriented and [001]-textured samples, respectively. P was calculated using the $I_{T(hkl)}$ obtained from the XRD patterns of the [001]-textured samples, and P_0 was calculated using the $I_{R(hkl)}$ obtained from the XRD patterns of the untextured samples.

The XRD patterns of the samples were analyzed by Rietveld refinement using the FullProf suite program. The microstructures of the samples were studied using scanning electron microscopy (FE-SEM; Hitachi, S-4800). The orientations of the grains in the textured samples were analyzed using EBSD (JEOL, JSM-7500F). The domain structures were studied using TEM (Hitachi, H-9000). The d_{33} values of the samples were measured using a d_{33} meter (Micro-Epsilon Channel Product, DT-3300, USA), and the $\varepsilon^{T}_{33}/\varepsilon_0$, dielectric loss (*tan* δ), and electromechanical coupling factor (k_p) were obtained using an impedance analyzer (Agilent Technologies, HP 4194A, USA). Polarization versus electric field (*P–E*) hysteresis curves and current density versus electric field (*J–E*) loops were measured using a ferroelectric tester (RT66C, Precision, USA) with a high-voltage amplifier (Trek, 610E). The strain versus electric field (*S–E*) loops were measured using a laser displacement sensor (aix-ACCT System GmbH,

Aachen, Germany). The *P*–*E* and *S*–*E* loops were recorded at 1 Hz in silicon oil.

2. Rietveld refinement of the XRD patterns obtained for the NKNS-0.02SZ-0.02BAZ + *y* mol% NN thick films with *y* = 0.0 and 5.0

Figure S1 shows the Rietveld refinement of the XRD patterns of the untextured NKNS-0.02SZ-0.02BAZ thick film ($y = 0.0$). The crystal structure of this thick film was identified as an R-O-T multi-structure that comprises *R3m* rhombohedral (25.3%), *Amm2* orthorhombic (55.7%), and *P4mm* tetragonal (19.0%) structures. The XRD pattern of the textured NKNS-0.02SZ-0.02BAZ + *y* mol% NN thick film with $y = 5.0$ is displayed in Fig. S2. The crystal structure of this thick film can be identified as a mixture of *R3m* rhombohedral (24.8%), *Amm2* orthorhombic (55.5%), and *P4mm* tetragonal (19.7%) structures. Therefore, this thick film has a R-O-T structure. The atomic coordinates, lattice parameters, and *R* values of the models of the NKNS-0.02SZ-0.02BAZ + *y* mol% NN thick films with $y = 0.0$, and 5.0 are listed in Table S1. The above-mentioned results indicate that the NKNS-0.02SZ-0.02BAZ + *y* mol% thick films ($x = 0.02$ and $0.0 \leq y \leq 5.0$) have the same R-O-T structure with similar proportions of the R, O, and T structures. Further, the NKNS-0.02SZ-0.02BAZ piezoceramic has an R-O-T structure. Therefore, it can be concluded that the addition of NN seeds did not change the crystal structure of the NKNS-0.02SZ-0.02BAZ piezoceramic.

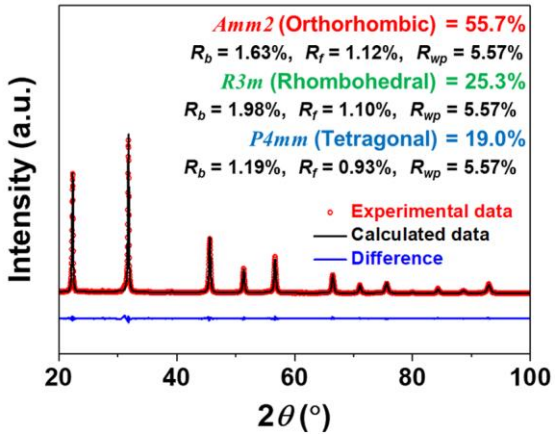

Figure S1. Rietveld refinement of the XRD pattern obtained for the untextured NKNS-0.02SZ-0.02BAZ thick film (y = 0.0).

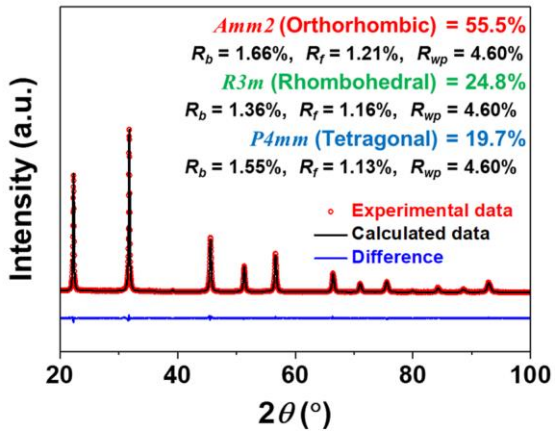

Figure S2. Rietveld refinement of the XRD pattern obtained for the textured NKNS-0.02SZ-0.02BAZ + 5.0 mol% NN thick film (y = 5.0).

Table S1. Parameters calculated from the Rietveld refinement of the XRD data of the NKNS-0.02SZ-0.02BAZ + *y* mol% NN thick films with *y* = 0.0 and 5.0.

NN content	Structural model (SG)	Site label	x	y	z	Lattice parameter [Å]	*R* factor [%]
y = 0.0	Orthorhombic (*Amm2*) 55.7%	K/Na/Sr/Bi/Ag Nb/Sb/Zr O1 O2	0(-) 0.500(-) 0(-) 0.500(-)	0(-) 0(-) 0(-) 0.260(10)	0(-) 0.518(12) 0.545(20) 0.291(18)	a = 3.9686(3) b = 5.6324(3) c = 5.6333(3) α = β = γ = 90°	$R_p/R_{wp}/R_{exp}$ R_b/R_f 3.84/5.57/3.04 1.63/1.12
	Rhombohedral (*R3m*) 25.3%	K/Na/Sr/Bi/Ag Nb/Sb/Zr O	0(-) 0(-) 0.511(-)	0(-) 0(-) –0.511(-)	0.483(6) 0(-) 0.484(-)	a = b = 5.6280(3) c = 6.9013(7) α = β = 90° γ = 120°	$R_p/R_{wp}/R_{exp}$ R_b/R_f 3.84/5.57/3.04 1.98/1.10
	Tetragonal (*P4mm*) 19.0%	K/Na/Sr/Bi/Ag Nb/Sb/Zr O1 O2	0(-) 0.500(-) 0.500(-) 0.500(-)	0(-) 0.500(-) 0.500(-) 0(-)	0(-) 0.564(8) 0.104(19) 0.661(19)	a = b = 3.9732(2) c = 3.9778(2) α = β = γ = 90°	$R_p/R_{wp}/R_{exp}$ R_b/R_f 3.84/5.57/3.04 1.19/0.93
y = 5.0	Orthorhombic (*Amm2*) 55.5%	K/Na/Sr/Bi/Ag Nb/Sb/Zr O1 O2	0(-) 0.500(-) 0(-) 0.500(-)	0(-) 0(-) 0(-) 0.225(11)	0(-) 0.501(8) 0.465(11) 0.314(14)	a = 3.9715(3) b = 5.6349(2) c = 5.6358(2) α = β = γ = 90°	$R_p/R_{wp}/R_{exp}$ R_b/R_f 3.40/4.60/3.16 1.66/1.21
	Rhombohedral (*R3m*) 24.8%	K/Na/Sr/Bi/Ag Nb/Sb/Zr O	0(-) 0(-) 0.511(-)	0(-) 0(-) –0.511(-)	0.470(5) 0(-) 0.484(-)	a = b = 5.6279(2) c = 6.9012(6) α = β = 90° γ = 120°	$R_p/R_{wp}/R_{exp}$ R_b/R_f 3.40/4.60/3.16 1.36/1.16
	Tetragonal (*P4mm*) 19.7%	K/Na/Sr/Bi/Ag Nb/Sb/Zr O1 O2	0(-) 0.500(-) 0.500(-) 0.500(-)	0(-) 0.500(-) 0.500(-) 0(-)	0(-) 0.575(8) 0.086(14) 0.643(14)	a = b = 3.9758(2) c = 3.9804(2) α = β = γ = 90°	$R_p/R_{wp}/R_{exp}$ R_b/R_f 3.40/4.60/3.16 1.55/1.13

3. *P-E* hysteresis curves and *J-E* loops obtained for the NKNS-0.02SZ-0.02BAZ + *y* mol% NN thick films with ($1.0 \leq y \leq 5.0$)

Figures S3(a)-(c) show the *P–E* hysteresis curves obtained for the NKNS-0.02SZ-0.02BAZ + *y* mol% NN thick films ($1.0 \leq y \leq 5.0$). The variation in the P_S values with increasing *y* was insignificant; however, the P_r value increased with an increase in *y*, and the maximum value was obtained at $y = 3.0$ (Fig. 3(b)); this slightly decreased for the thick film with $y = 5.0$ (Fig. S3(c)). The increase in P_r was expected to improve the piezoelectricity of the thick film because the piezoelectric constant increased with an increase in polarizability. Further, the E_C value of the thick film with $y = 1.0$ was ~0.54 kV/mm (Fig. S3(a)), and it slightly decreased to 0.49 kV/mm for the thick film with $y = 5.0$, as shown in Fig. S3(c). The decrease in E_C was expected to increase the piezoelectricity of the thick film because poling is easy when E_C is small. The thick film with $y = 3.0$ shows the largest P_r and a small E_C, which indicates that this thick film has good piezoelectric characteristics. Figures S3(a-c) show the *J–E* loops of the NKNS-0.02SZ-0.02BAZ + *y* mol% NN thick films ($1.0 \leq y \leq 5.0$). Two peaks were found in all thick films because of the conventional domain switching with the application of an electric field. Therefore, it can be concluded that these thick films exhibited good ferroelectric properties.

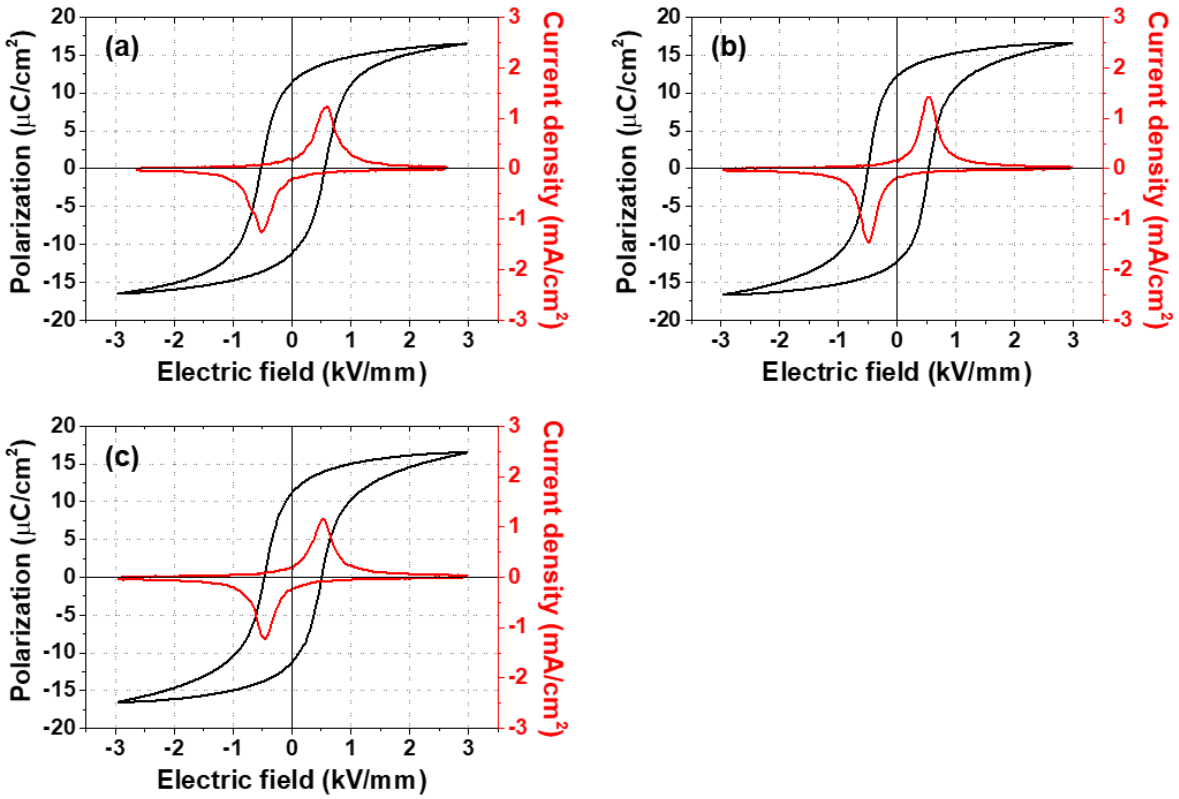

Figure S3. *P-E* hysteresis curves and *J-E* loops obtained for the NKNS-0.02SZ-0.02BAZ + *y* mol% NN thick films: (a) *y* = 1.0, (b) *y* = 2.0, and (c) *y* = 5.0.

4. The ε_r versus temperature curves obtained for the NKNS-0.02SZ-0.02BAZ + y mol% NN thick films with ($1.0 \leq y \leq 5.0$)

The ε_r versus temperature curves obtained for the NKNS-0.02SZ-0.02BAZ + y mol% NN thick films ($1.0 \leq y \leq 5.0$) are shown in Fig. S4(a-c). The T_C and $T_{O\text{-}T}$ of the thick film with y = 1.0 are approximately 158 and 44 °C, respectively; they slightly decrease with an increase in y to 150 and 40 °C, respectively, for the thick film with y = 5.0. The NN seeds may not completely and homogeneously diffuse into the matrix of the thick film during sintering, which can cause the compositions of the textured thick films to differ slightly. Therefore, the slight decrease in T_C and $T_{O\text{-}T}$ with increasing y for the NKNS-0.02SZ-0.02BAZ + y mol% NN thick films can be explained by the slight compositional difference of the thick films.

Figures S4(d)-(h) show the ε_r versus temperature curves measured at various frequencies near T_C obtained for the NKNS-0.02SZ-0.02BAZ + y mol% NN thick films ($0.0 \leq y \leq 5.0$). For the thick film with y = 0.0, the T_C increased very slightly upon increasing the frequency; the difference between the T_C measured at the maximum frequency and that at the minimum frequency (ΔT) was small (~1 °C) (Fig. S4(a)). Therefore, the relaxor properties of this thick film were considered to be small. The ΔT value of the NKNS-0.02SZ-0.02BAZ + y mol% NN thick films increased with increasing y, and the thick film with y = 5.0 showed the largest ΔT value of ~6 °C. Therefore, the relaxor properties increase with an increase in the NN content, and this can be attributed to the presence of the stress between the NN seeds and the matrix [3,4]. The broadening of the T_C peak with an increase in y can be explained by the increase in the relaxor properties with an increase in NN content.

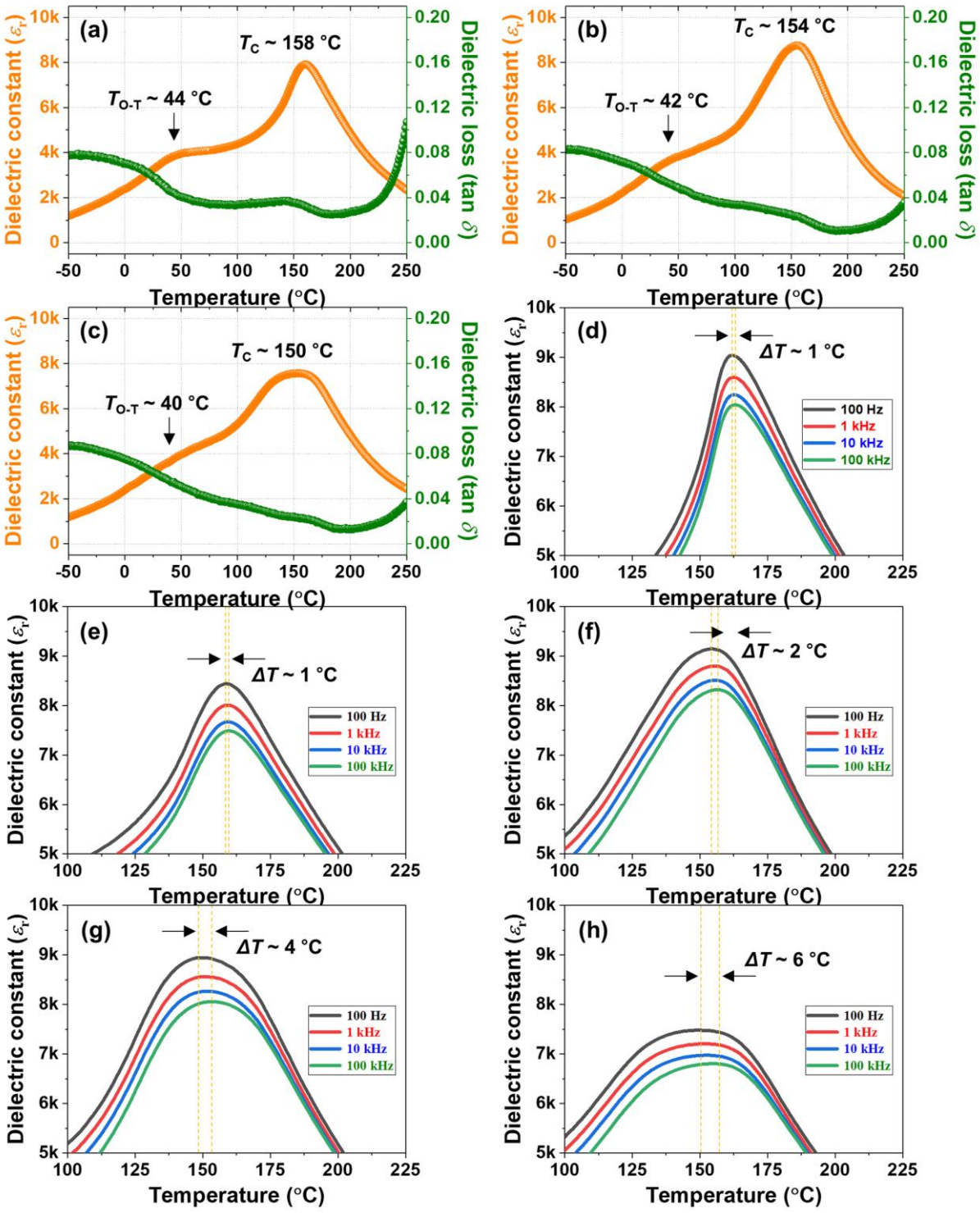

Figure S4. The ε_r versus temperature curves obtained for the NKNS-0.02SZ-0.02BAZ + y mol% NN thick films: (a) y = 1.0, (b) y = 2.0, and (c) y = 5.0. The ε_r versus temperature curves measured at various frequencies for the NKNS-0.02SZ-0.02BAZ + y mol% NN thick films: (d) y = 0.0, (e) y = 1.0, (f) y = 2.0, (g) y = 3.0, and (h) y = 5.0.

5. SEM images of the NKNS-(0.04-x)SZ-xBAZ thick films ($0.0 \leq x \leq 0.04$)

The microstructure of the NKNS-(0.04-x)SZ-xBAZ thick films ($0.0 \leq x \leq 0.04$) were investigated using SEM, as shown in Figures S5(a)-(d). The thick film with $x = 0.0$ has a relatively dense microstructure containing large grains with an average grain size of ~23 μm and these grains are well aligned along the [001] direction, as shown in Fig. S5(a). A similar microstructure was also observed for the other thick films (Figs. S5(b)-(d)). Rectangular holes indicated by arrows were observed in the thick films, which were formed due to the diffusion of NN seeds into the matrix of the thick films. These holes have been frequently observed in NKN-based thick films textured using NN seeds [2,5].

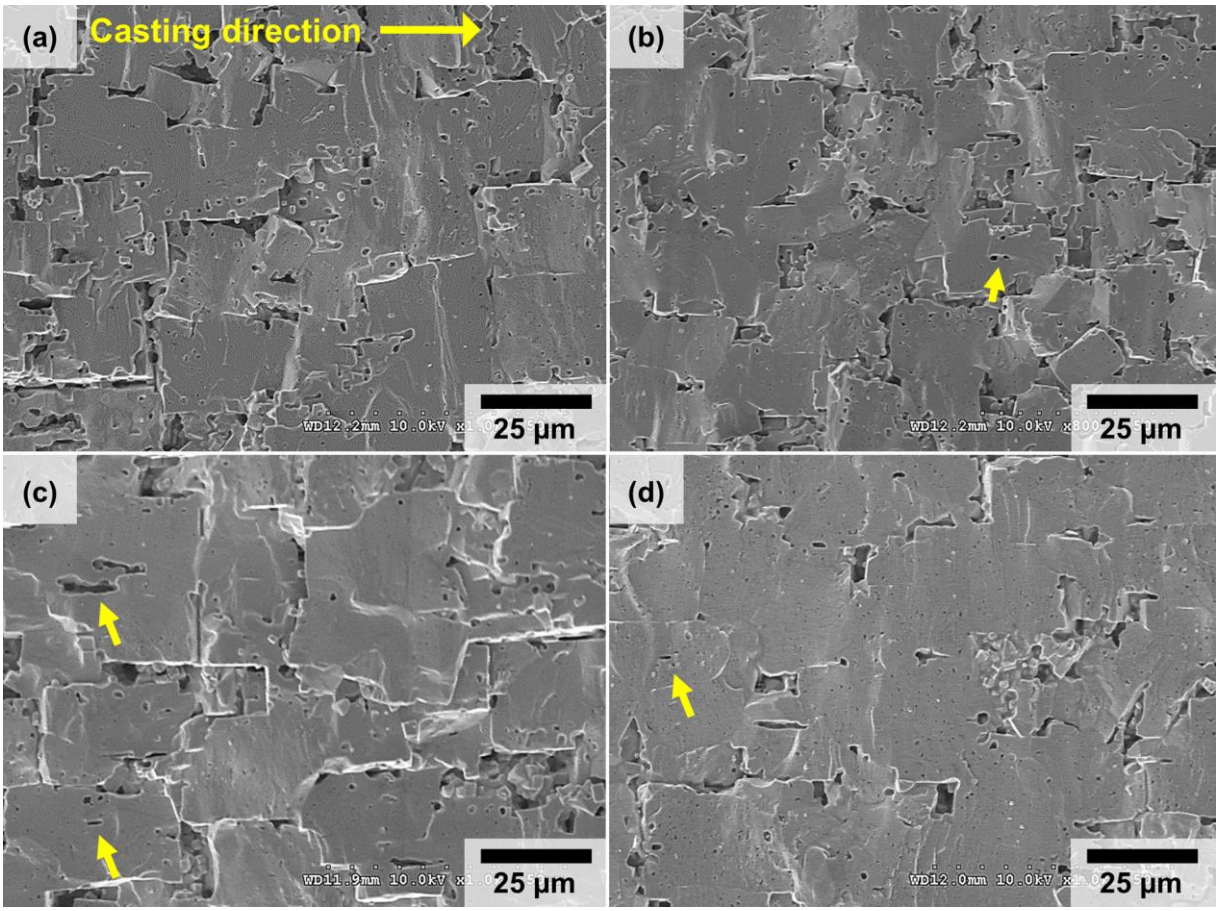

Figure S5. SEM images of the textured NKNS-(0.04-x)SZ-xBAZ + 3.0 mol% NN thick films: (a) $x = 0$, (b) $x = 0.01$, (c) $x = 0.025$, and (d) $x = 0.04$.

6. Rietveld refinement of the XRD patterns obtained for the textured NKNS-SZ + 3.0 mol% NN thick film

The XRD pattern obtained for the NKNS-SZ (x = 0.0) thick film textured using 3.0 mol% NN seeds was analyzed using Rietveld analysis, as shown in Fig. S6. An R-O model was used for the analysis. This model shows a small R_{wp} (5.48), which was slightly larger than that of the R-O-T model (5.37) (Fig. 6(a)). Therefore, it has been suggested that the textured NKNS-SZ thick film has an R-O-T structure. However, this R-O-T structure is very similar to the R-O structure because the proportion of the tetragonal structure is small. In addition, the atomic coordinates, lattice parameters, and R values of this R-O model of the thick film are listed in Table S2.

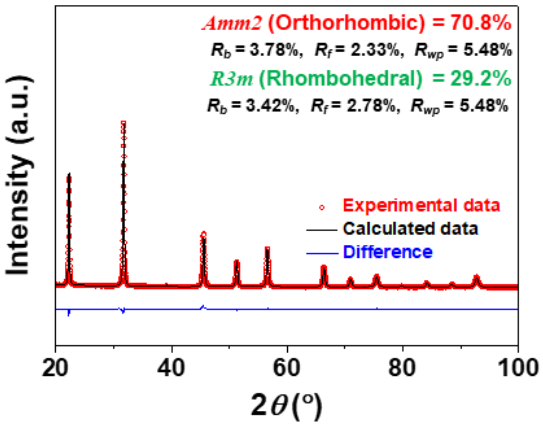

Figure S6. Rietveld refinement of the XRD pattern obtained for the NKNS-SZ thick film using an R-O model.

Table S2. Parameters calculated from the Rietveld refinement of the R-O model of the NKNS-SZ thick film.

BAZ content	Structural model (SG)	Site label	x	y	z	Lattice parameter [Å]	*R* factor [%]
x = 0.0	Orthorhombic (*Amm2*) 70.8%	K/Na/Sr/Bi/Ag	0(-)	0(-)	0(-)	a = 3.9759(2)	$R_p/R_{wp}/R_{exp}$
		Nb/Sb/Zr	0.500(-)	0(-)	0.483(7)	b = 5.6374(2)	R_b/R_f
		O1	0(-)	0(-)	0.492(15)	c = 5.6389(2)	4.20/5.48/3.25
		O2	0.500(-)	0.287(7)	0.249(13)	α = β = γ = 90°	3.78/2.33
	Rhombohedral (*R3m*) 29.2%	K/Na/Sr/Bi/Ag	0(-)	0(-)	0.476(4)	a = b = 5.6317(2)	$R_p/R_{wp}/R_{exp}$
		Nb/Sb/Zr	0(-)	0(-)	0(-)	c = 6.9106(5)	R_b/R_f
		O	0.511(-)	–0.511(-)	0.517(5)	α = β = 90°	4.20/5.48/3.25
						γ = 120°	3.42/2.78

7. *P-E* hysteresis curves and *J-E* loops obtained for the textured NKNS-(0.04-x)SZ-xBAZ thick films ($0.0 \leq x \leq 0.04$)

Figures S7(a)-(f) show the *P-E* hysteresis curves and *J-E* loops obtained for the NKNS-(0.04-x)SZ-xBAZ thick films ($0.0 \leq x \leq 0.04$) textured using 3.0 mol% NN seeds. The P_S, P_r, and E_C values of the thick films are shown in Fig. S7(g). The P_S and P_r values of the thick film with $x = 0.0$ was approximately 16.9 and 12.9 μC/cm^2, respectively. The P_S value slightly decreased with an increase in x; however, the variation was not significant. A slightly decreased P_S value of 16.6 μC/cm^2 was observed for the thick film with $x = 0.04$. The variation in P_r was not significant for thick films with $x \leq 0.02$. However, the P_r value decreases when x is > 0.02, and the thick film with $x = 0.04$ has a reduced P_r value of 11.5 μC/cm^2. The decrease in the P_r value can be explained by the increase in the proportion of the T structure as the sample with the T structure generally exhibits a decreased P_r value [6]. The E_C value of the thick film with $x = 0.0$ was ~0.49 kV/mm, and its variation with an increase in x was negligible for the thick films with $x \leq 0.02$. However, it increased to 0.59 kV/mm for the thick film with $x = 0.04$ because of the increase in the proportion of the T structure. The *J–E* loops obtained for the thick films are illustrated in Figs. S7(a)-(f), and all thick films show two peaks because of the conventional domain switching upon the application of an electric field; this confirms that they have the characteristics of normal ferroelectric ceramics.

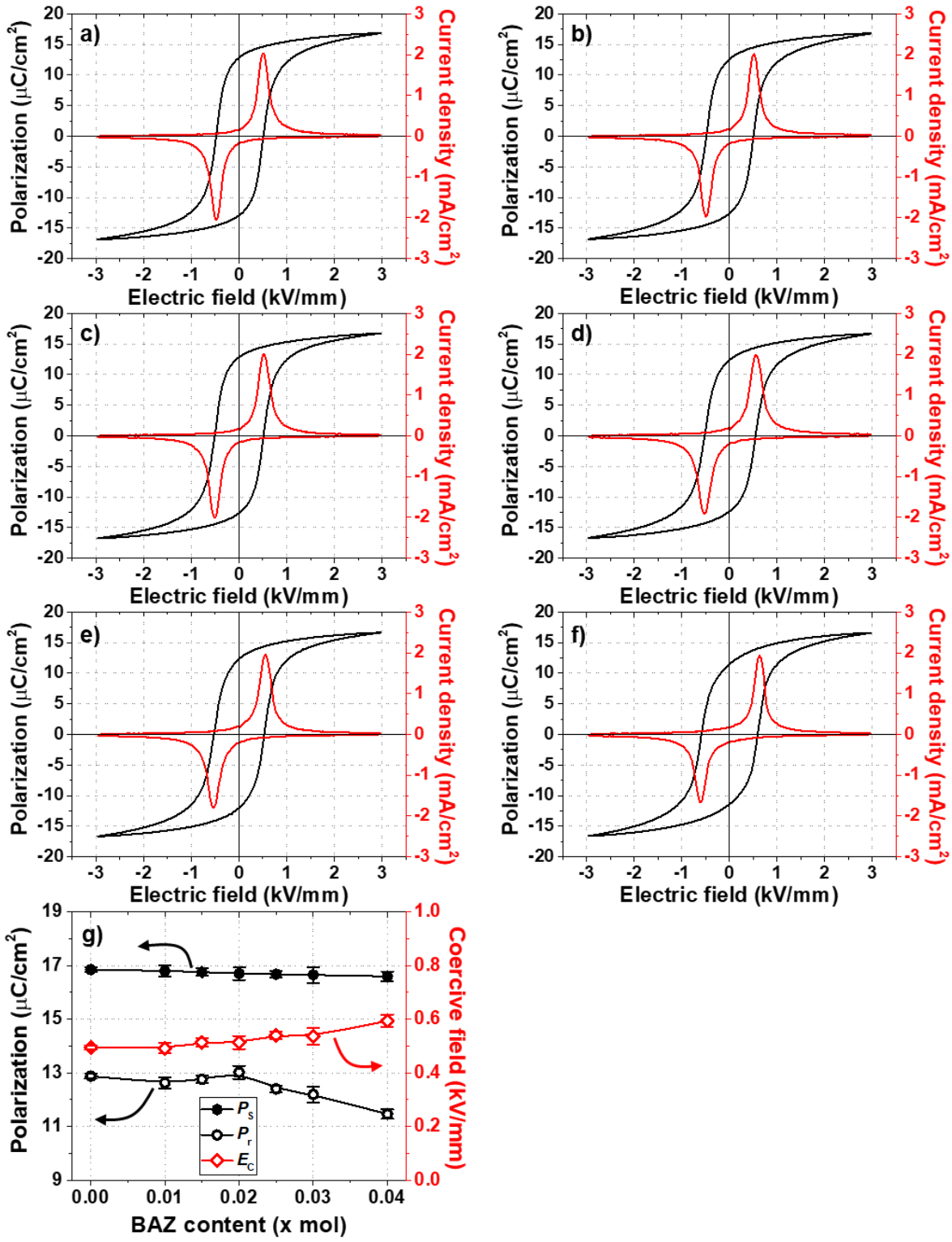

Figure S7. *P-E* hysteresis curves and *J-E* loops obtained for the textured NKNS-(0.04-x)SZ-xBAZ thick films: (a) $x = 0.0$, (b) $x = 0.01$, (c) $x = 0.0125$, (d) $x = 0.025$, (e) $x = 0.03$ and (f) $x = 0.04$. (g) P_S, P_r and E_C values of the thick films studied.

8. Relationship between the proportion of R-O structure and the k_p^T/k_p^{UT} value

Figure S8 shows the proportion of the R-O structure in the textured NKNS-(0.04-x)SZ-xBAZ thick films ($0.0 \leq x \leq 0.04$) and the k_p^T/k_p^{UT} values, where k_p^T and k_p^{UT} are the k_p values of the textured thick films and the untextured piezoceramics, respectively. The proportion of the R-O structure is > 80% for the thick films ($0.0 \leq x \leq 0.02$), which showed a large k_p^T/k_p^{UT} value of ~1.15. However, a relatively small k_p^T/k_p^{UT} value (< 1.04) was observed for the thick films with $x = 0.03$ and 0.04, which was attributed to the proportion of the R-O structure being small (< 56%). Similar results were also observed for the d_{33} value, as shown in Fig. 8(d).

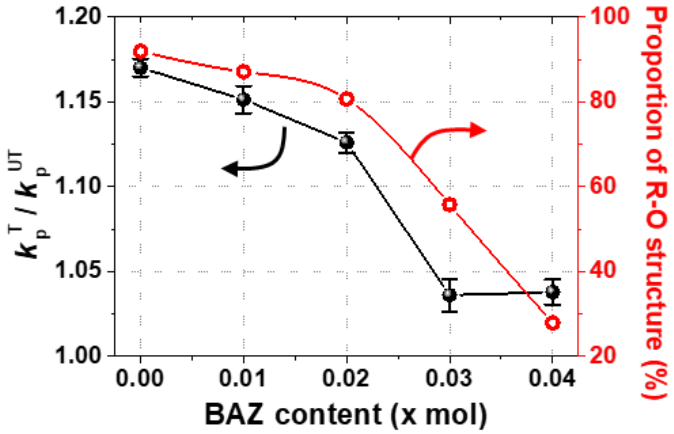

Figure S8. Proportion of the R-O structure and k_p^T/k_p^{UT} values obtained for the NKNS-(0.04-x)SZ-xBAZ thick films ($0.0 \leq x \leq 0.04$).

9. Relationship between the d_{15}/d_{33} of single crystal grown along the polar direction and the d_{33} of single crystals grown along the [001] direction

According to previous studies, a piezoelectric single crystal with an O structure, which is grown along the [110] polar direction, generally shows a large d_{15}/d_{33} value (or shear piezoelectric constant) with an applied electric field along the [110] polar direction [7]. Furthermore, when this orthorhombic single crystal is grown along the [001] direction, the four P_Ss were aligned along the <110> directions, as shown in Fig. S9(a). When an electric field is applied along the [001] growth direction, four P_Ss increase the polarization along the [001] through rotational motion (Fig. S9(a)) [8,9]. Because the orthorhombic single crystal has a large shear piezoelectric constant (d_{15}/d_{33} value), the four P_Ss can be easily rotated, resulting in a large d_{33} value [7,10]. The rhombohedral single crystal also shows a large d_{15}/d_{33} value when it was grown along the [111] polar direction [7]. Therefore, the rhombohedral single crystal grown along the [001] direction also showed a large d_{33} value due to its large d_{15}/d_{33} value, which also assists the rotation of four P_Ss aligned along the [111] direction, as shown in Fig. S9(b) [11,12]. However, it has been reported that the d_{15}/d_{33} value of a single crystal with a T structure is relatively small [3,8,11]. Therefore, it can be concluded that a single crystal with the O (or R) structure, which is grown along the [001] direction, can have a large d_{33} value due to the large d_{15}/d_{33} value. Furthermore, it can be suggested that this principle can also be applied to [001]-textured piezoelectric thick films with multiple structures because the [001]-textured thick film is similar to the single crystal grown along the [001] direction.

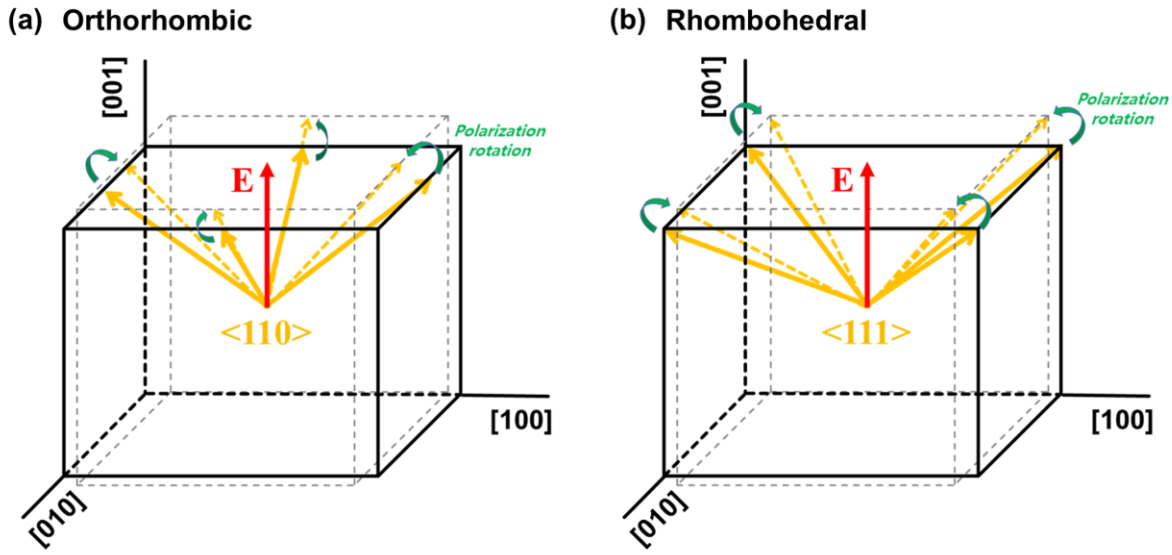

Figure S9. The *P*ss developed in the single crystal grown along the [001] direction with an (a) orthorhombic and (b) rhombohedral structures. The rotation of *P*ss, which is induced by the application of the electric field along the [001] direction, is indicated using green arrows.

References

[1] F. Lotgering, Topotactical reactions with ferrimagnetic oxides having hexagonal crystal structures—I, *J. inorg. nucl.*, **1959**, 9(2), 113-123. https://doi.org/10.1016/0022-1902(59)80070-1

[2] D.S. Kim, J.M. Eum, S.H. Go, H.S. Shin, H. Kim, S.J. Chae, S.W. Kim, E.J. Kim, J.U. Woo, S. Nahm, Remarkable piezoelectric performance and good thermal stability of <001>-textured $0.96(K_{0.5}Na_{0.5})(Nb_{1-y}Sb_y)O_3$-$0.04SrZrO_3$ lead-free piezoelectric ceramics, *J. Alloys Compd.*, **2021**, 160662. https://doi.org/10.1016/j.jallcom.2021.160662

[3] Y. Liu, Y. Chang, F. Li, B. Yang, Y. Sun, J. Wu, S. Zhang, R. Wang, W. Cao, Exceptionally high piezoelectric coefficient and low strain hysteresis in grain-oriented (Ba, Ca)(Ti, Zr)O_3 through integrating crystallographic texture and domain engineering, ACS *Appl. Mater. Interfaces*, **2017**, 9(35), 29863-29871. https://doi.org/10.1021/acsami.7b08160

[4] X. Gao, N. Dong, F. Xia, Q. Guo, H. Hao, H. Liu, S. Zhang, Impact of phase structure on piezoelectric properties of textured lead-free ceramics, *Crystals*, **2020**, 10(5), 367. https://doi.org/10.3390/cryst10050367

[5] A. Hussain, A. Maqbool, J.S. Kim, T.K. Song, M.H. Kim, W.J. Kim, S.S. Kim, Sodium excess Ta-Modified $(K_{0.5}Na_{0.5})NbO_3$ ceramics prepared by reactive template grain growth method, *Int. J. Appl. Ceram. Technol.*, **2015**, 12(1), 228-234. https://doi.org/10.1111/ijac.12150

[6] E.J. Kim, T.G. Lee, D.S. Kim, S.W. Kim, Y.J. Yee, S.H. Han, H.W. Kang, S. Nahm, Textured Pb(Zr,Ti)O_3-Pb[$(Zn,Ni)_{1/3}Nb_{2/3}$]O_3 multilayer ceramics and their application to piezoelectric actuators, *Appl. Mater. Today*, **2020**, 20, 100695. https://doi.org/10.1016/j.apmt.2020.100695

[7] M. Davis, M. Budimir, D. Damjanovic, N. Setter, Rotator and extender ferroelectrics: Importance of the shear coefficient to the piezoelectric properties of domain-engineered crystals and ceramics, *J. Appl. Phys.*, **2007**, 101(5), 054112. https://doi.org/10.1063/1.2653925

[8] F. Li, S. Zhang, D. Lin, J. Luo, Z. Xu, X. Wei, T.R. Shrout, Electromechanical properties of $Pb(In_{1/2}Nb_{1/2})O_3$–$Pb(Mg_{1/3}Nb_{2/3})O_3$–$PbTiO_3$ single crystals, *J. Appl. Phys.*, **2011**, 109(1), 014108. https://doi.org/10.1063/1.3530617

[9] S. Wada, K. Muraoka, H. Kakemoto, T. Tsurumi, H. Kumagai, Enhanced piezoelectric properties of potassium niobate single crystals by domain engineering, *Jpn. J. Appl. Phys.*, **2004**, 43(9S), 6692. https://doi.org/10.1143/JJAP.43.6692

[10] F. Li, S. Zhang, Z. Xu, X. Wei, T.R. Shrout, Critical property in relaxor-$PbTiO_3$ single crystals–shear piezoelectric response, *Adv. Funct. Mater*., **2011**, 21(11), 2118-2128. https://doi.org/10.1002/adfm.201002711

[11] S.E. Park, T.R. Shrout, Relaxor based ferroelectric single crystals for electro-mechanical actuators, *Mater. Res. Innov*., **1997**, 1(1), 20-25. https://doi.org/10.1007/s100190050014

[12] R. Zhang, W. Cao, Transformed material coefficients for single-domain $0.67Pb(Mg_{1/3}Nb_{2/3})O_3$–$0.33PbTiO_3$ single crystals under differently defined coordinate systems, *Appl. Phys. Lett.*, **2004**, 85(26), 6380-6382. https://doi.org/10.1063/1.1842365